Magnetic structure of the Laves phase compound $TiFe_2$



1992 J. Phys.: Condens. Matter 4 10015

(http://iopscience.iop.org/0953-8984/4/49/028)

J. Phys.: Condens. Matter 4 (1992) 10015–10024. Printed in the UK

# Magnetic structure of the Laves phase compound $TiFe_2$

P J Brown†, J Deportes‡ and B Ouladdiaf†

† Institut Laue–Langevin, 156X, 38042 Grenoble Cédex, France
‡ Laboratoire Louis Néel, CNRS, 166X, 38042 Grenoble Cédex, France

Received 3 September 1992

**Abstract.** The magnetic structure of $TiFe_2$ which crystallizes with the C15 Laves phase structure has been determined from neutron diffraction measurements made on both single-crystal and polycrystalline samples. In the antiferromagnetic structure the Fe2 atoms in the (6h) sites with the same $z$ coordinate are coupled ferromagnetically with the moments in successive layers alternately parallel and antiparallel to the $c$-axis. The Fe1 atoms which are in the (2a) sites are at an anti-centre of symmetry and carry no ordered moment. Magnetization measurements support this structure, giving a positive paramagnetic Curie temperature and showing the metamagnetic transition characteristic of ferromagnetically coupled sheets. Polarized neutron measurements indicate that in the antiferromagnetic phase the two types of Fe atom contribute almost equally to the susceptibility and suggest that the magnetic moment on the Fe1 atoms is only induced by the molecular field due to the aligned moment on the surrounding Fe2 atoms.

## 1. Introduction

A great deal of experimental and theoretical work has been carried out recently on the magnetic properties of the $AB_2$ Laves phase compounds. A large number of compounds can be formed by varying the A and B elements, and a wide range of different behaviour has been observed.

Among Laves phase compounds, those in which A is a transition metal of the 3d, 4d, or 5d series, and B is one of the later members of the 3d series, are of particular interest with respect to their magnetic properties. The $AFe_2$ compounds with A = Sc, Ti, Nb, Hf, Ta have been extensively studied mainly by magnetization and Mössbauer techniques. The compounds $ScFe_2$ [1], and $HfFe_2$ [2] show ferromagnetic behaviour, while $TiFe_2$ [3] is antiferromagnetic. $NbFe_2$ [4] is a weak itinerant antiferromagnet and $TaFe_2$ [5] is paramagnetic at all temperatures. However, in the pseudobinary system $Hf_{1-x}Ta_xFe_2$ [6], there is a first-order phase transition between ferromagnetic and antiferromagnetic states. In $Ti_{1-x}Sc_xFe_2$ with $x < 0.3$, a mixed ferromagnetic/antiferromagnetic state has been found and the transition between this mixed state and the antiferromagnetic state has been observed [7]. This very varied magnetic behaviour has been successfully explained using the spin fluctuation theory of Moriya and Usami [8].

The bulk magnetic properties of the Laves phase compound $TiFe_2$ have been reported to be very sensitive to deviation from stoichiometry [3]. The iron-rich materials become ferromagnetic whereas the titanium-rich materials show antiferromagnetic behaviour. This dependence of the magnetic properties on the

0953-8984/92/4910015+10$07.50  

stoichiometry is due to substitution of Fe atoms in Ti sites. Wertheim *et al* [9] have shown by Mössbauer measurements that stoichiometric $TiFe_2$ is antiferromagnetic below $T_N = 275$ K. They deduced that only one of the two independent sets of Fe atoms, those on the (6h) site ($Fe_2$), are magnetically ordered.

In this paper we present results obtained by magnetization measurements and neutron diffraction experiments on both polycrystalline and single-crystal samples of $TiFe_2$.

## 2. Experiments and results

The $AFe_2$ compounds crystallize in the C15 cubic Laves phase $MgCu_2$-type structure when A = Y, Zr or a rare earth, and in the C14 hexagonal Laves phase $MgZn_2$-type structure when A = Sc, Ti, Nb, Hf or Ta. In the hexagonal structure (space group $P6_3/mmc$), the A atoms occupy a single crystallographic site (4f), whereas there are two non-equivalent sites types (2a) and (6h) for the Fe atoms which are labelled Fe1 and Fe2 respectively. The atomic positions and local symmetry are detailed in table 1.

**Table 1.** Crystallographic parameters of the hexagonal Laves phase structure ($P6_3/mmc$).

| Atom | Size | Site symmetry | Atomic positions | |
|---|---|---|---|---|
| Fe1 | 2a | $\bar{3}m$ | $(0,0,0)$; $(0,0,\frac{1}{2})$ | |
| Fe2 | 6h | $mm$ | $\pm(x,\ x,\ \frac{1}{4})$ | $x = -\frac{1}{6}$ |
| | | | $\pm(2x,\ x,\ \frac{1}{4})$ | |
| | | | $\pm(x,\ 2x,\ \frac{1}{4})$ | |
| Ti | 4f | $3m$ | $\pm(\frac{1}{3},\ \frac{2}{3},\ z)$ | $z = \frac{1}{16}$ |
| | | | $\pm(\frac{1}{3},\ \frac{2}{3},\ \frac{1}{2} - z)$ | |

A polycrystalline sample at the exact stoichiometric composition $TiFe_2$ was prepared using the cold-crucible method in a high-frequency induction furnace. No phase other than $TiFe_2$ with the C14 hexagonal structure was detected by x-ray analysis. The single-crystal sample was grown by the Czochralski method also in a high-frequency induction furnace.

### *2.1. Magnetostatic studies*

The magnetization measurements on polycrystalline samples were carried out in the temperature range 2–800 K using fields up to 80 kOe. High-field magnetization measurements up to 200 kOe have also been carried out on a single-crystal sample orientated with the field parallel and perpendicular to the hexagonal axis in the temperature range 4–300 K.

The magnetization of the polycrystalline sample shows a linear dependence on the applied magnetic field at all temperatures in the range 2–800 K. The thermal variation of the magnetic susceptibility and its inverse are shown in figure 1. The magnetic susceptibility has a maximum at $T_N = 280$ K, the Néel temperature of the compound. Above $T_N$ it follows a Curie–Weiss law with a paramagnetic Curie temperature $\Theta_P = 150$ K. Figure 2 shows the dependence of the magnetization of the single-crystal

sample on the magnetic field at 4 K. It shows a strong magnetocrystalline anisotropy; when the magnetic field is applied in the basal plane the magnetization increases linearly without saturating up to 200 kOe, whereas when the field is applied along the c-axis a metamagnetic-type transition is observed at a critical field $H_c = 180$ kOe. The magnetization has the same value at 190 kOe regardless of the field direction. The critical field $H_c$ decreases linearly with increasing temperature.

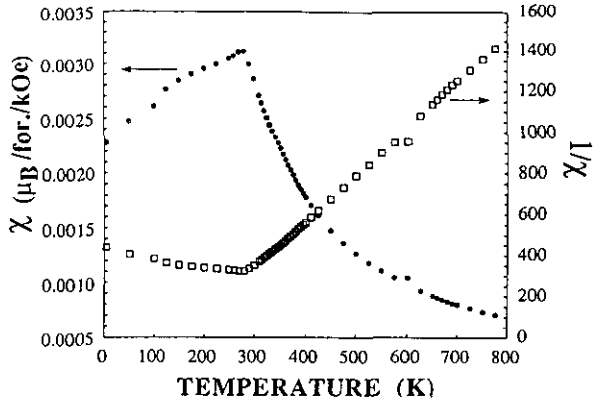


**Figure 1.** Thermal variation of the magnetic susceptibility and its inverse for the $TiFe_2$ polycrystalline sample.

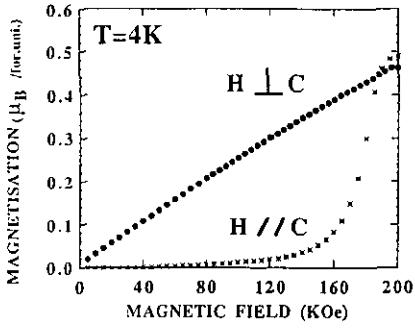


**Figure 2.** Field dependence of the magnetization parallel and perpendicular to the c-axis for single-crystal $TiFe_2$ at 4 K.

### *2.2. Powder neutron diffraction studies*

Powder neutron diffraction experiments were performed using a multidetector spectrometer with a neutron wavelength $\lambda = 2.496$ Å at the Grenoble Nuclear Centre. The refinement of the magnetic and nuclear structures at different temperatures was performed using a Rietveld refinement method. In order to eliminate the texture problem, we used a very fine powder (50 $\mu$m) which was mixed with aluminium powder. The contamination of the spectra by Al reflections was not large. Indeed in

the range of scattering angle used in the experiments ($2\theta < 110°$), only two Bragg peaks (200 and 111) of Al are observed. Several diffraction patterns were collected between 4 and 300 K. Those obtained at 300 K and 4 K are shown in figure 3.

The pattern at 300 K is characteristic of the nuclear Bragg reflections associated with the $MgZn_2$-type structure and was used to refine the structural parameters. The scattering lengths used in the refinement were $b_{Ti} = -0.344 \times 10^{-12}$ cm, $b_{Fe} = 0.954 \times 10^{-12}$ cm. The adjustable $z$ coordinate of Ti at the 4f site and the $x$ coordinate of Fe2 at the 6h site obtained were $z = 0.0647(9)$ and $x = -0.1705(2)$. These differ significantly from the values given in the literature. In figure 3 the full curves represent the calculated pattern, the points the observed one, the short vertical lines the Bragg positions and the lower curves the difference between observations and calculations. Excellent agreement is obtained. The reliability factor $R = \sum |I_{obs} - I_{cal}| / \sum I_{obs}$ was 3%.

Below the Néel temperature (figure 3(*b*), $T = 4$ K), the patterns are characterized by the increase of the intensity of some Bragg peaks due to the magnetic contribution to the diffraction pattern. This increase is easily observed in the 200 reflection which is almost zero at room temperature. In the space group $P6_3/mmc$ the reflections $hh$–$2h\ell$ with odd $\ell$ are systematically absent so another important feature is the appearance of a small peak indexed as 111. However the peaks with a similar form 001 and 003 were not observed.

The thermal variation of the lattice parameters deduced from the neutron diffraction patterns collected at different temperatures is shown in figure 4. Below $T_N$, they show an anomalous thermal variation: the $c$ parameter increases with decreasing temperature while the $a$ parameter decreases. No significant anomaly was observed in the thermal variation of the volume, nor was there any evidence for loss of hexagonal symmetry.

### *2.3. Single-crystal diffraction measurements with unpolarized neutrons*

Measurements of the integrated intensities of reflections for unpolarized neutrons were made using the D15 diffractometer which is placed on one of the inclined thermal beams at the high-flux reactor of the Institut Laue–Langevin. The diffractometer is equipped with a detector which can be inclined to the omega axis and was used in normal beam geometry. Two different single crystals cut from the ingot were used. They had dimensions 10 and 2 $mm^3$ and were mounted in turn on the diffractometer, inside a variable temperature cryostat. The larger was aligned with a $\langle 010 \rangle$ axis and the smaller with a $\langle \bar{1}10 \rangle$ axis, parallel to the omega axis.

$Q$-scans along the reciprocal lattice directions [001], [$h$00], [$hh$0] at 4.2 K for the larger crystal gave no evidence for scattering away from the reciprocal lattice points. There was, however, an increase by a factor of about eight in the intensity of the 200 reflection on cooling from ambient temperature to 100 K. These observations agree with the powder diffraction measurements and suggest that the magnetic and chemical cells have the same size, so the magnetic propagation vector is [000]. The temperature dependence of the intensity of the 200 reflection is shown in figure 5; it drops to a small constant value above 280 K indicating an antiferromagnetic transition in agreement with the susceptibility measurements. Since with zero propagation vector magnetic and nuclear scattering occurs in the same reflections a good knowledge of the nuclear structure is needed in order to be able to separate nuclear from magnetic scattering. For this reason integrated intensities were measured above and below the

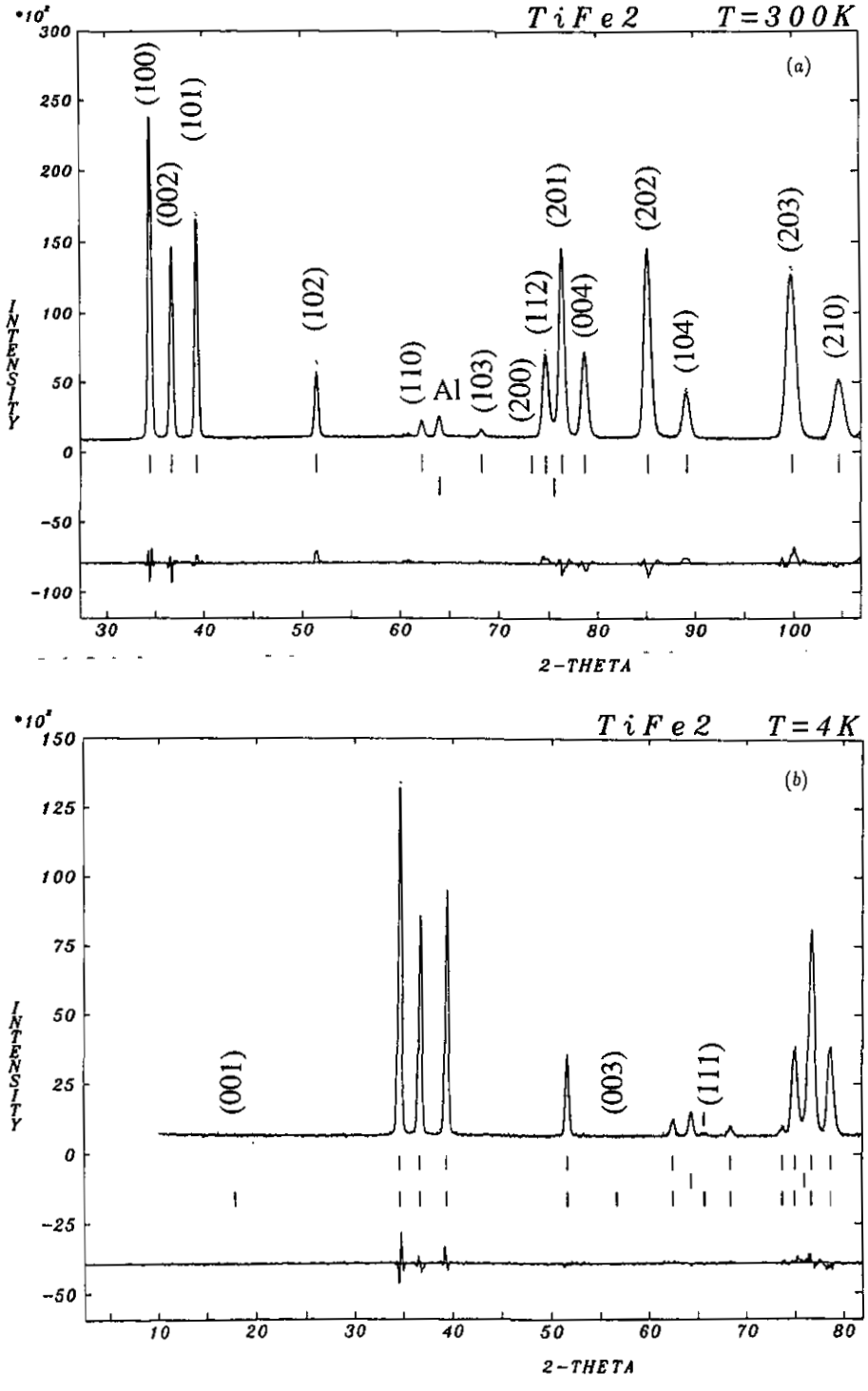


**Figure 3.** Powder neutron diffraction patterns with $\lambda = 2.496$ Å: (*a*) $T = 300$ K, (*b*) $T = 4$ K. The full curves are the calculated data, and the lower curves show the difference between observations and calculations.

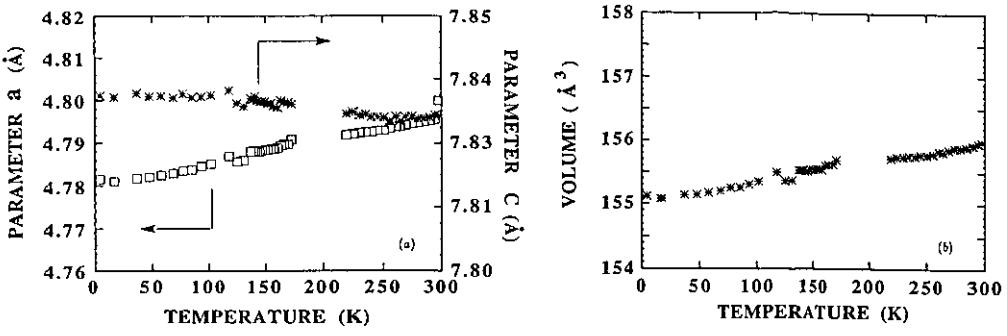


**Figure 4.** Thermal dependence of the hexagonal lattice parameters of $TiFe_2$ deduced from the powder neutron data: (*a*) *a* and *c* parameters; (*b*) Volume, *v*.

**Table 2.** Summary of the integrated intensity measurements performed on the single-crystal sample.

| Sample orientation | Wavelength (Å) | Temperature (K) | Maximum sin $\theta/\lambda$ (Å$^{-1}$) | Number of independent reflections |
|---|---|---|---|---|
| ⟨010⟩ | 1.176 | 300 | 0.75 | 110 |
| ⟨010⟩ | 1.176 | 4.3 | 0.75 | 184 |
| ⟨010⟩ | 0.854 | 300 | 0.50 | 48 |
| ⟨1$\bar{1}$0⟩ | 1.176 | 300 | 0.60 | 48 |
| ⟨1$\bar{1}$0⟩ | 1.176 | 90 | 0.60 | 48 |

Néel temperature for both crystals and at two wavelengths (1.176 Å and 0.864 Å). A summary of the measurements made is given in table 2.

A preliminary analysis of the data collected at ambient temperature showed evidence for extinction and for multiple scattering; this latter effect was shown up by significant intensity measured in reflections of the form $hh{-}2h\ell$ with $\ell$ odd which should be absent for space group $P6_3/mmc$ and which were not seen in the powder patterns. An empirical correction for multiple scattering at low temperatures was made using the assumption that it would be unchanged on lowering the temperature, and that all the differences between the observed and calculated intensities for the nuclear structure at ambient temperature are due to multiple scattering. To this end a joint refinement of all data collected at ambient temperature was made including as variables the two positional parameters, three temperature factors, a scale factor for each set of data and a single mosaic spread parameter to describe extinction in the Becker–Coppens model [10]. The agreement between observed and calculated structure factors obtained was quite good ($R = 3\%$) so long as the systematically absent reflections were omitted. The most significant differences otherwise were in the weakest reflections. The parameters obtained from the refinement are in excellent agreement with those obtained from the powder data.

### *2.4. Polarized neutron measurements*

Measurements with polarized neutrons were made on the smaller of the two crystals used for the integrated intensity measurements. The crystal was mounted in

a variable temperature insert in a superconducting magnet on the D3 polarized neutron diffractometer at ILL. Initially it was orientated so that the [001] axis was perpendicular to the field and a ⟨010⟩ axis was approximately parallel to it. Measurements of polarized neutron flipping ratios were made at a temperature of 100 K in an applied field of 4.6 T. All reflections of the form $hk\ell$ with $k = 0, 1$ were measured to a limit of $\sin\theta/\lambda = 0.75$ Å$^{-1}$. A second set of data was measured in the same conditions but with the crystal mounted with [001] parallel to the field. The magnetic scattering observed with this sample orientation was much weaker and measurements were limited to $(hk0)$ reflections with $\sin\theta/\lambda < 0.5$ Å$^{-1}$.

Magnetic structure factors for the magnetization aligned by the field were calculated from the flipping ratios, making corrections for imperfect polarization and for extinction, using the structural and extinction parameters obtained from the analysis of the integrated intensity measurements.

## 3. Determination of the magnetic structure

### *3.1. The magnetic arrangement*

The magnetization measurements show that the magnetic arrangement is antiferromagnetic. The positions of the magnetic peaks observed in both the powder and single-crystal measurements then put severe constraints on the possible magnetic structures. Firstly the magnetic cell is the same as the crystallographic one hence the magnetic propagation vector $\kappa = [000]$. Next, the presence of the 111 reflection indicates that the glide plane perpendicular to ⟨110⟩ reverses the spin direction. Finally the absence of the 001 and 003 magnetic reflections suggests that the spin direction is along the $c$-axis. The only structure which retains hexagonal symmetry, and which is consistent with these observations, is that illustrated in figure 6. It has been taken as the basis for refinements based on the powder and single-crystal data both of which led to satisfactory agreement between observed and calculated magnetic intensities. In this arrangement the moments of Fe2 atoms in the same layer ($z = \frac{1}{4}$) are ferromagnetically aligned while the magnetic coupling between adjacent layers is antiferromagnetic. The resultant molecular field at the Fe1 site is zero as it lies midway between two antiferromagnetically coupled planes on a centre of symmetry which is associated with time reversal. Under these circumstances the Fe1 atoms can have no ordered moment.

### *3.2. Refinement of the magnetic structure*

The powder neutron diffraction patterns at 300 K (figure 3($a$)) were collected in the scattering angle range 27–107° in $2\theta$ to obtain the maximum number of nuclear reflections; however, those at 2 K (figure 3($b$)) were collected in the range 2.5–82.5° and thus contain the maximum number of measurable magnetic reflections. Figure 7 shows that part of the patterns between 50 and 80° on a large scale, and shows clearly the appearance of the 111 reflection. The antiferromagnetic structure deduced in section 3.1 is very simple so the number of parameters to be refined is very small: just the magnetic moment of the Fe2 atoms for the single-crystal data, with the addition of the lattice parameters in the powder refinement. Excellent agreement was obtained between the observations and the calculations for both the powder and the single-crystal diffraction data. The value obtained for the Fe2 moment was $1.4(1)\mu_B$ at 4 K.

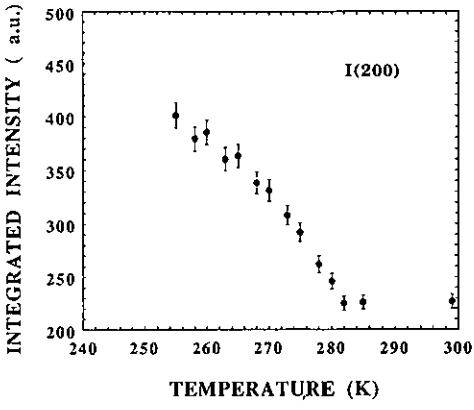


**Figure 5.** Thermal variation of the integrated intensity of the 200 reflection obtained from $TiFe_2$ single-crystal diffraction measurements.

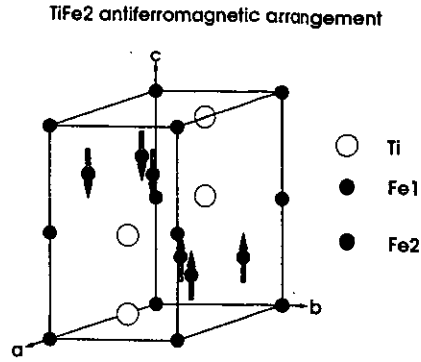


**Figure 6.** Magnetic structure of $TiFe_2$ deduced from powder and single-crystal diffraction experiments.

## 4. Analysis of the polarized neutron data

The magnetic scattering by the magnetization induced by the applied field was compared with that calculated for a simple model consisting of superposition of spherical magnetization distributions as calculated for the $Fe^{2+}$ free ion [11] centred at the iron sites. The magnitudes of the moment associated with the Fe1 and Fe2 sites in this model were obtained from least-squares fits of the calculated structure factors to the observations. For both orientations the susceptibility of the two sites was found to be approximately equal, but the absolute value of the moment induced, by the applied field of 4.6 T, for the $c$-axis orientation (0.008(2) $\mu_B$/atom) was ten times smaller than that obtained with the $c$-axis perpendicular to the field (0.095(5)$\mu_B$/atom).

## 5. Discussion

The magnetic structure deduced from the neutron diffraction studies allows the metamagnetic transition observed in the single-crystal magnetization data to be understood. In fact, this metamagnetic behaviour is equivalent to a 'spin flop' except that the exchange energy is too large compared to the magnetic anisotropy energy for the usual 'spin flop' transition observed in compounds like $FeCl_2$ to take place. The spin structure can be described as a stacking of strongly coupled ferromagnetic layers with weak antiferromagnetic interactions between layers. This is consistent with the observed positive paramagnetic temperature of 150 K.

The lack of an ordered moment on the Fe1 atoms is worthy of some comment. Similar absence of moment on particular 3d sites has been found in some Mn Laves phase compounds such as the cubic compound $TbMn_2$ [12]. This feature is always associated with structures in which there are sites at which the magnetic symmetry imposes zero molecular field. That such structures can be stable is associated with close approach of the Mn–Mn distance to that leading to instability of the 3d Mn moment, and to topological frustration which severely restricts the number of possible antiferromagnetic structures. In $TiFe_2$ the fact that a site with no ordered moment

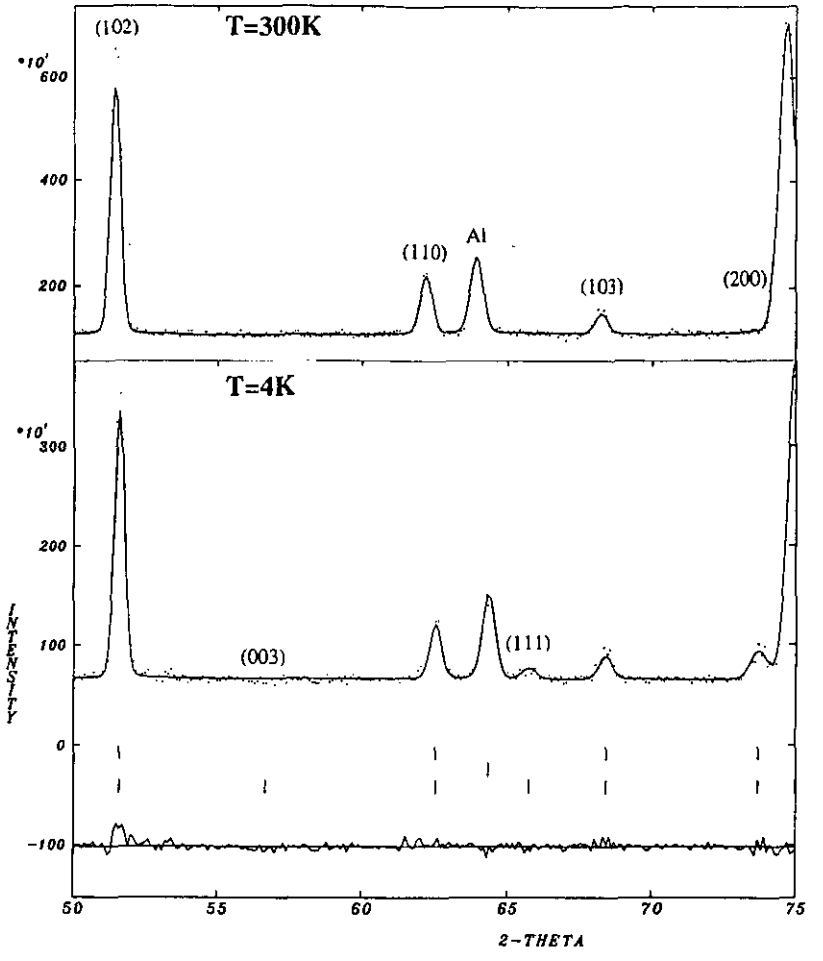


**Figure 7.** A part of the powder diffraction patterns between 50 and 80° on a large scale, showing the appearance of the 111 and 200 reflections.

persists down to low temperatures suggests that the Fe moment also is near to instability in this compound. The Fe1 atom would then be non-magnetic rather than magnetically disordered. Such an assumption leads to a consistent interpretation of the induced moments obtained from the polarized neutron measurements. The observation that the moment induced on Fe2 by a field parallel to $c$ is about ten times smaller than that induced in the perpendicular plane is consistent with the susceptibility measurements and is a measure of the strength of the antiferromagnetic coupling. The similar behaviour of the moment induced on Fe1 is hard to understand if its moment is simply disordered. If, however, moment at this site is induced only by the resultant molecular field of the surrounding Fe2 atoms then its proportionality to the aligned Fe2 moment is simply explained.

Asano and Ishido [13] have recently calculated the density of states at different sites in $TiFe_2$. They have used the linear muffin tin orbital method within the framework of the local spin density approximation. From the local density of states,

making the assumption that only the Fe2 atoms carry a moment and that it is parallel to $c$, they have estimated its magnitude as $1.4\mu_B$/Fe2, in amazingly good agreement with our results.

## Acknowledgments

The authors would like to thank Dr E Ressouche from the CENG for his assistance in the powder neutron diffraction experiment.

## References

[1] Ikeda K, Nakamichi T, Yamada T and Yamamoto M 1974 *J. Phys. Soc. Japan* **36** 611
[2] Takamich T, Kai K, Aoki Y, Ikeda K and Yamamoto M 1970 *J. Phys. Soc. Japan* **29** 794
[3] Nakamichi T 1968 *J. Phys. Soc. Japan* **25** 1189
[4] Yamada Y and Sakata A 1988 *J. Phys. Soc. Japan* **57** 46
[5] Kai K, Nakamichi T and Yamamoto M 1970 *J. Phys. Soc. Japan* **29** 1094
[6] Nishihara Y and Yamagushi Y 1983 *J. Phys. Soc. Japan* **52** 3630
[7] Nishihara Y and Yamagushi Y 1986 *J. Phys. Soc. Japan* **55** 920
[8] Moriya T and Usami K 1977 *J. Phys. Soc. Japan* **23** 935
[9] Wertheim G K, Wernick J H and Sherwood R C 1969 *Solid State Commun.* 7 1399
[10] Becker P and Coppens P 1974 *Acta Crystallogr.* A **30** 129
[11] Watson R E and Freeman A J 1961 *Acta Crystallogr.* **14** 27
[12] Brown P J, Ouladdiaf B, Ballou R, Deportes J and Markosyan A S 1992 *J. Phys.: Condens. Matter* **4** 1103
[13] Asano S and Ishida S 1988 *J. Phys. F: Met. Phys.* **18** 501